Proceedings of the ASME 2020
International Mechanical Engineering Congress and Exposition
IMECE2020
November 16-19, 2020, Virtual, Online

IMECE2020-23328

INVESTIGATING THE PRECIPITATION KINETICS AND HARDENING EFFECTS OF γ" IN INCONEL 625 USING A COMBINATION OF MESO-SCALE PHASE-FIELD SIMULATIONS AND MACRO-SCALE PRECIPITATE STRENGTHENING CALCULATIONS

Caleb O. Yenusah[1,2], Yanzhou Ji[3], Yucheng Liu[1,2,*], Tonya W. Stone[1,2]
[1]Department of Mechanical Engineering, Mississippi State University, Mississippi State, MS 39762, USA
[2]Center for Advanced Vehicular Systems, Mississippi State University, Mississippi State, MS 39762, USA
[3]Department of Materials Science and Engineering, The Pennsylvania State University, University Park, PA 16801 USA

Mark F. Horstemeyer[4], Lei Chen[5]
[4]School of Engineering, Liberty University, Lynchburg, VA 24515, USA
[5]Department of Mechanical Engineering, University of Michigan-Dearborn, Dearborn, MI 48128, USA

ABSTRACT

Precipitation strengthening of alloys by the formation of secondary particles (precipitates) in the matrix is one of the techniques used for increasing the mechanical strength of metals. Understanding the precipitation kinetics such as nucleation, growth, and coarsening of these precipitates is critical for evaluating their hardening effects and improving the yield strength of the alloy during heat treatment. To optimize the heat treatment strategy and accelerate alloy design, predicting precipitate hardening effects via numerical methods is a promising complement to trial-and-error-based experiments and the physics-based phase-field method stands out with the significant potential to accurately predict the precipitate morphology and kinetics. In this study, we present a phase-field model that captures the nucleation, growth, and coarsening kinetics of precipitates during isothermal heat treatment conditions. Thermodynamic data, diffusion coefficients, and misfit strain data from experimental or lower length-scale calculations are used as input parameters for the phase-field model. Classical nucleation theory is implemented to capture the nucleation kinetics. As a case study, we apply the model to investigate γ" precipitation kinetics in Inconel 625. The simulated mean particle length, aspect ratio, and volume fraction evolution are in agreement with experimental data for simulations at 600 ℃ and 650 ℃ during isothermal heat treatment. Utilizing the meso-scale results from the phase-field simulations as input parameters to a macro-scale coherency strengthening model, the evolution of the yield strength during heat treatment was predicted. In a broader context, we believe the current study can provide practical guidance for applying the phase-field approach as a link in the multiscale modeling of material properties.

Keywords: Phase-field model; Precipitation kinetics; Isothermal aging; Nickel-base alloys; *γ"*

NOMENCLATURE

η	order parameter
X_i	composition of i^{th} solute
T	temperature
V_m	molar volume
$f^{\gamma/\gamma"}$	Gibbs free energy of γ or $\gamma"$ phase
k	gradient energy coefficient
C_{ijkl}	elastic constants
ϵ_{ij}^0	misfit strain tensor between γ and $\gamma"$
ϵ_{ij}	total strain
α	free energy penalty constant
σ	interfacial energy
M_i	chemical mobility of i^{th} solute
D_i	diffusivity of i^{th} solute
D_0	diffusion prefactor
Q_d	diffusion activation energy
R	ideal gas constant
L	kinetic coefficient

* Contact author: liu@me.msstate.edu

Δt	time step
l_0	grid size
E_0	reference energy
J	nucleation rate

1. INTRODUCTION

The properties of a material are dictated by its microstructure, which are in turn dependent on the processing conditions. Therefore, knowledge of the evolution of microstructure during processing is important in correctly predicting the mechanical properties of the resulting material. Precipitation strengthening is one of the techniques used for increasing the mechanical strength of metals. The process uses heat treatment to facilitate the formation of secondary particles (precipitates) in the metal's grains structure that help hinder the motion of dislocation, or defects in a crystal's lattice and thereby strengthening the alloy [1]. Precipitation kinetics can be divided into nucleation, growth and coarsening stages [2]. During the nucleation stage, nuclei of the precipitating phase form in the supersaturated matrix due to spatially localized composition fluctuation. The growth stage is categorized by the diffusional growth of a precipitate by solute transfer from the surrounding matrix without competing with the growth of other particles. After sufficient depletion of the solute in the matrix during the growth stage, the free growth of individual precipitates ceases, and the coarsening regime starts. During coarsening, the growth of larger particles continues at the expense of smaller particles which dissolve due to diffusive mass transfer from smaller particles to larger ones.

Experimental and theoretical understanding of each stage of the precipitation process is critical for evaluating precipitate hardening effects and improving the yield strength of the alloy during heat treatment. To optimize the heat treatment strategy and accelerate alloy design, predicting precipitate hardening effects via theoretical analysis or computer simulations is a promising complement to trial-and-error-based experiments, making it possible to efficiently explore the whole heat treatment design space, reducing the alloy development time and cost. The ability to determine the precipitate hardening effects significantly relies on the correct prediction of the evolution of precipitate morphology, size, volume fraction, and spatial distribution during heat treatment. Different models have been developed to concurrently capture all stages of precipitation reaction. Most prominent among them are Kampmann & Wagner Numerical (KWN) method [2], Svoboda-Fischer-Fratzl-Kozeschnik (SFFK) framework [3], Johnson-Mehl-Avrami-Kolmogorov (JMAK) kinetics [4], and Phase-field method [5].
One of the advantages of the phase-field method compared to the rest, is its capability to accurately predict complex morphological evolution of precipitates without any presumption on their shape or mutual distribution. This is because the general formulation of the phase-field model allows for the inclusion of all energy terms that contributes to the evolution of the precipitate such as interfacial, elastic, and chemical energy. Such a generalized formulation makes the phase-field method a valuable tool for bridging different length scales in the multiscale modeling of the process-structure-property relation in materials [6-8].

In this study, we present a phase-field model that captures the nucleation, growth, and coarsening kinetics of precipitates during isothermal heat treatment conditions. Thermodynamic data, diffusion coefficients, and misfit strain data from experimental or lower length-scale calculations are used as input parameters for the model. Classical nucleation theory is implemented to capture the nucleation kinetics. As a case study, we apply the model to investigate γ'' precipitation kinetics in Inconel 625, a commercial Ni-based superalloy widely used in the aerospace, chemical processing, nuclear, and oil/gas industries, due to its high strength; outstanding fatigue, corrosion, and oxidation resistance; and excellent fabricability and weldability [9] The results from the meso-scale phase-field simulations were utilized in a macro-scale coherency strengthening model to predict the evolution of yield strength during heat treatment.

2. MATERIALS AND METHODS

2.1 Phase-field method

Inconel 625 is a complex multi-component alloy. To save computational efforts while capturing the essential features of the precipitation process, we used a pseudo-ternary (Ni-Al_x-Nb_y) CALPHAD thermodynamic database developed for Ni-based superalloys [10]. Only the strengthening precipitate in Inconel 625 (γ'') will be considered in this work. The system was represented with two composition fields, X_{Al^*} and X_{Nb^*}. Two orientation variants of γ'' out of the three were consider in the 2D phase-field simulations. Two antiphase domains were introduced for each γ'' variant to reduce coalescence events between the same variant during the growth and coarsening stages. Therefore, γ'' is represented by four order parameters, $\{\eta_1, \eta_2, \eta_3, \eta_4\}$. The temperature dependent free energy functional for the system can then be expressed as:

$$F = \int_V \left[f_{bulk}\left(X_{Al^*}, X_{Nb^*}, \eta_p, T\right) + f_{grad}\left(\nabla \eta_p\right) + e_{el} \right] dV \qquad (1)$$

where f_{bulk} is the bulk free energy density of the system, f_{grad} is the gradient energy due to the inhomogeneous distribution of the order parameters, and e_{el} is the elastic strain energy density. They are respectively defined as:

$$f_{bulk}\left(X_{Al^*}, X_{Nb^*}, \{\eta_p\}, T\right) = V_m^{-1} \cdot \left[1 - \sum_{p=1}^{4} h\left(n_p\right) \right] \cdot f^{\gamma}\left(X_{Al^*}^{\gamma}, X_{Nb^*}^{\gamma}, T\right) + V_m^{-1} \cdot \left[1 - \sum_{p=1}^{4} h\left(n_p\right) \right] \cdot f^{\gamma''}\left(X_{Al^*}^{\gamma''}, X_{Nb^*}^{\gamma''}, T\right) + g\left(\{n_p\}\right) \qquad (2)$$

$$f_{grad} = \sum_{p=1}^{4} \frac{k_p}{2} \left(\nabla \eta_p\right)^2 \qquad (3)$$

$$e_{el} = \frac{1}{2} C_{ijkl} \left(\epsilon_{ij} - \epsilon_{ij}^0\right)\left(\epsilon_{kl} - \epsilon_{kl}^0\right) \qquad (4)$$

where $h(\eta_p) = 2\eta_p^2 - \eta_p^4$ is an interpolation function and $g(\{n_p\})$ is a Landau-type double-well function expressed as:

$$g(\{\eta_p\}) = w^{\gamma''} \cdot \sum_{p=1}^{4} \eta_p^2 (1 - |\eta_p|)^2 + \alpha \cdot \sum_{p \neq q}^{4} \eta_p^2 \eta_q^2 \quad (5)$$

Cahn-Hilliard [11] and Allen-Cahn [12] equations are solved to obtain the spatial and temporal evolution of the concentration fields and order parameters, respectively:

$$\frac{\partial X_i}{\partial t} = \nabla \cdot \left(M_i \nabla \frac{\partial f^{\gamma}}{\partial X_i^{\gamma}} \right), \; i = Al^*, Nb^* \quad (6)$$

$$\frac{\partial \eta_p}{\partial t} = -L \left(\frac{\partial f_{bulk}}{\partial \eta_p} - k_p \nabla^2 \eta_p + \frac{\partial e_{el}}{\partial \eta_p} \right) \quad (7)$$

where M_i $(i = Al^*, Nb^*)$ are the chemical mobilities of Al^* and Nb^*, respectively. The mobilities can be estimated as $M_i = \frac{D_i}{V_m \frac{\partial^2 f^{\gamma}}{\partial X_i^2}}$, where $D_i = D_0 exp\left(\frac{-Q_d}{RT}\right)$ $(i = Al^*, Nb^*)$ are the temperature dependent diffusivities of Al^* and Nb^*. L is the kinetic coefficient for structural evolution. These governing equations are normalized by the simulation grid size l_0 and reference energy E_0 and solved numerically using the spectral method. All inputs parameters used for the phase-field simulations are provided in Table 1.

2.2 Nucleation kinetics

Nucleation is incorporated into the phase-field model using the method described by Simmons et al. [13]. The probability for nucleation at a simulation cell is defined as:

$$P = 1 - \exp(-J \cdot \Delta t) \quad (8)$$

where J is the nucleation rate which following the classical nucleation theory [14]. To determine numerically whether a particle nucleate locally or not in each time step, a random number is generated for each untransformed cell and nucleation occurs when the number is smaller than P.

TABLE 1: Parameters for phase-field simulations.

Parameters	Expression
V_m	$1.05 \times 10^{-5}\ m^3/mol$
$X_{Al^*}^0, X_{Nb^*}^0$	$0.0046, 0.0243$
D_{0Al^*}, D_{0Nb^*}	$8.8 \times 10^{-5}\ m^2/s$
Q_{Al^*}, Q_{Nb^*}	$320\ kJmol^{-1}, 282\ kJmol^{-1}$
σ	$140\ mJ/m^2$
l_0	$0.5\ nm$ at T = 600 ℃ $1.0\ nm$ at T = 650 ℃
E_0	$2.5\ GPa$
L	$\frac{L^* D}{E_0 l_0^2}$, $L^* = 10$ for all T
C_{11}, C_{12}, C_{44}	$C_{11} = 203\ GPa, C_{12} = 150\ GPa,$ $C_{44} = 135\ GPa$
ϵ_{ij}^0	$\begin{bmatrix} 0.0067 & 0 & 0 \\ 0 & 0.0067 & 0 \\ 0 & 0 & 0.0286 \end{bmatrix}$

3. RESULTS AND DISCUSSION

3.1 Phase-field simulations: γ'' morphology evolution and kinetics

Phase-field simulations were performed at 600 ℃ and 650 ℃ with grid sizes of 0.5nm and 1.0nm, respectively. The grid size was increased with temperature because the discretization time step in the simulation (Δt^*) is converted to real time through $\Delta t = \frac{(\Delta x)^2}{D_{Nb^*} \cdot \Delta t^*}$ and since larger particles are present at higher temperature, it is advantageous from a computational efficiency standpoint to increase the grid size with temperature, while maintaining a reasonable interfacial thickness. The 2D simulation cell size were $192\text{nm} \times 192\text{nm}$ and $256\text{nm} \times 256\text{nm}$ for 600 ℃ and 650 ℃, respectively. For each temperature, we performed six simulations with different random number generator seeds and averaged the results to reduce the statistical errors associated with the relatively small simulation size.

Figs. 1 and 2 show the simulated microstructure evolution of Inconel 625 aged at 600 ℃ and 650 ℃. Comparing these images with TEM images of aged samples (Figs. 5.8 and 5.10 in [15]), it is apparent that the phase-field simulation successfully reproduces the disk-shaped γ'' precipitates. The configurational arrangement of the precipitates by the simulation is also in agreement with experimental observation. Face-to-face coalesce between the same variant is rarely seen between the precipitates because of the elastic interaction between them. Instead, the precipitates tend to align/coalescence along their edges.

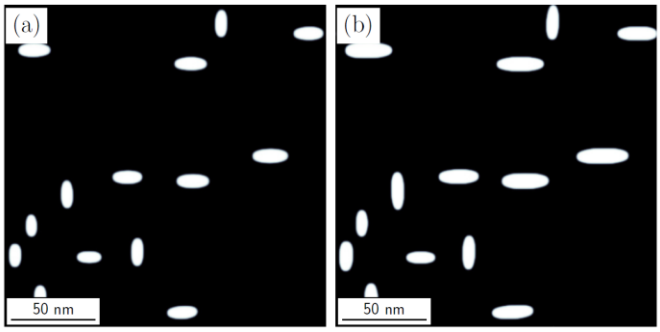

FIGURE 1: Phase-field simulation results for microstructure evolution of γ'' precipitates in Inconel 625 aged at 600 ℃ (a) after 1000 hours and (b) after 3000 hours.

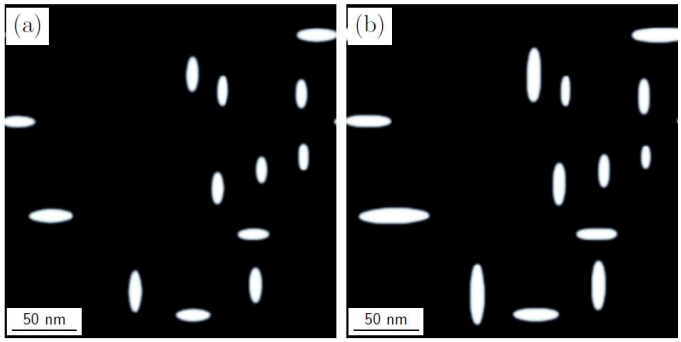

FIGURE 2: Phase-field simulation results for microstructure evolution of γ'' precipitates in Inconel 625 aged at 650 ℃ (a) after 200 hours and (b) after 1000 hours.

Figs. 3 and 4 show the evolution of mean particle length, aspect ratio, and volume fraction calculated from the phase-field simulations. The mean particle length, aspect ratio, and volume fraction are calculated from the aggregate of all particles from the six simulations with different random number generator seeds. The error bars in the simulation length and aspect ratio are calculated from their standard deviations. And the error bars in the volume fraction is calculated from the standard deviation between the six simulations. Generally, the simulated precipitate length and aspect ratio agree well with the experimental measurements. Although γ'' precipitates were assumed to nucleate as circular particles, because of the anisotropic misfit strain tensor between γ'' and γ matrix, the growth of the particles along the major axis is faster than the growth along the minor axis, resulting in the decrease of the aspect ratio (thickness/length) until an equilibrium value of about 0.3 is reached (Figs. 3b and 4b).

The equilibrium volume fraction was 6.3% for aging at 650 ℃ (Fig. 4c). However, for aging at 600 ℃, the equilibrium volume fraction is not yet reached even after about 4000 hours of aging. This is because of the sluggish growth of the particles at this temperature due to slower mobility of solute at lower temperatures. The growth and coarsening stages can be identified upon further examination of the volume fraction plots especially for samples aged at 650 ℃, for which the equilibrium volume fraction was reached. The growth stage is defined by a monotonic increase in both the volume fraction and length of the precipitates as the precipitates grow into the supersaturated matrix without competition between them. As the supersaturation in the matrix decreases and the composition in the matrix reached the equilibrium concentration, the free growth of each particle ceases and further increase in size is due to the transfer of mass from the smaller particles to the larger ones. From Fig. 4c, it can be observed that the growth stage lasted for about 300 hours and a transition period of about 500 hours ushered in the coarsening stage.

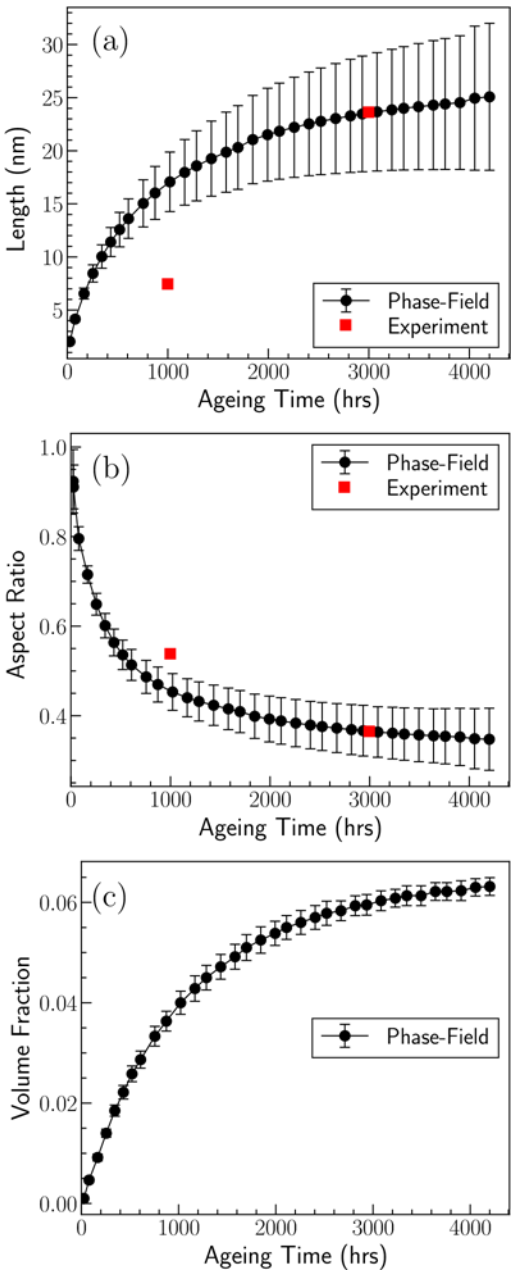

FIGURE 3: Simulated γ'' precipitation kinetics and comparison with experimental measurements [15] in Inconel 625 aged at 600 ℃. (a) Particle length. (b) Aspect ratio. (c) Volume fraction.

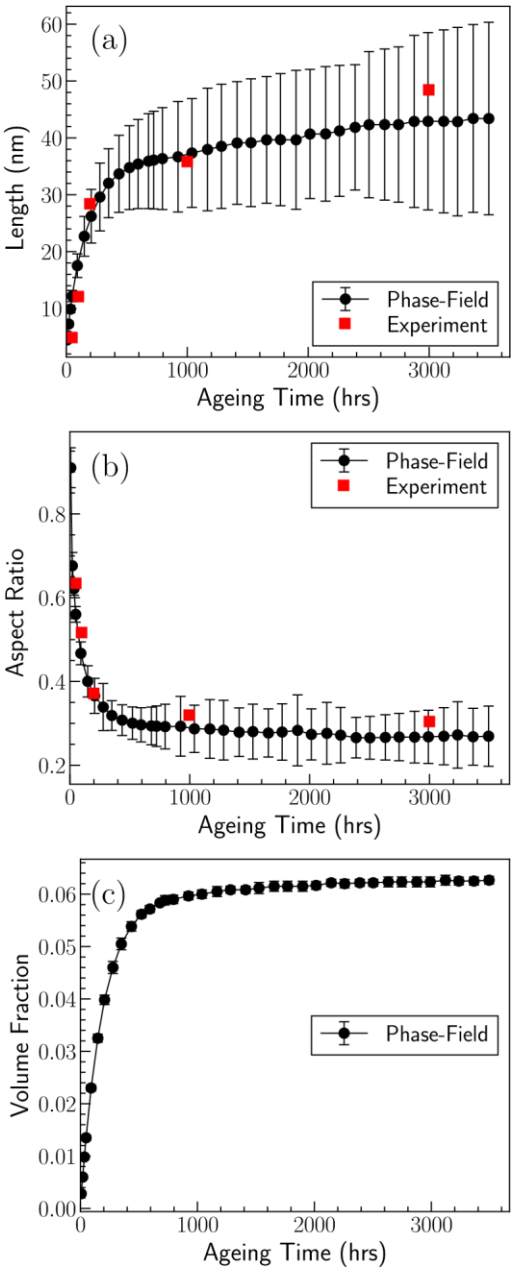

FIGURE 4: Simulated γ'' precipitation kinetics and comparison with experimental measurements [15] in Inconel 625 aged at 650 ℃. (a) Particle length. (b) Aspect ratio. (c) Volume fraction.

3.2 γ'' coherent strengthening

The main purpose of alloy aging is to increase the strength of the material through precipitation hardening. The increase in yield strength as a result of the coherent strengthening effect of γ'' can be calculated as [16]:

$$\sigma_{coherent} = 1.7MG|\epsilon|^{\frac{3}{2}}\left[\frac{h^2 f(1-\beta)}{2bR}\right]^{\frac{1}{2}} \quad (9)$$

where M is Taylor factor (3.06 for fcc materials), G is the shear modulus, ϵ is the tetragonal lattice misfit, f is the volume fraction of precipitates, R is the radius of the particles, h is the half thickness of the particles, β is a constant equals to $\frac{1}{3}$ when all the three variants are observed, and b is the magnitude of Burger's vector. We set $\epsilon = 0.0286$, $G = 77$ GPa, and $b = 2.54$ Å [16]. R, h, and f are functions of aging time and were obtained from the phase-field simulations. Substituting all the values into Eqn. (12), the coherent strengthening effect of γ'' as a function of aging time is calculated and plotted in Fig. 5. From the figure it can be observed that coherent strengthening increases with aging time until a maximum value is reached, after which over-aging results in the decrease of coherent strengthening. From Fig. 5, the strengthening response at 650 ℃ is much faster than at 600 ℃ because of the slower growth of the precipitates at 600 ℃. As a result, it takes about 2817 hours to reach the maximum strengthening of 599MPa at 600 ℃, compared to 722 hours to reach the maximum strengthening of 587MPa at 650 ℃. The properties of γ'' precipitates at the instance of maximum $\sigma_{coherent}$ for both aging temperatures is detailed in Table 2.

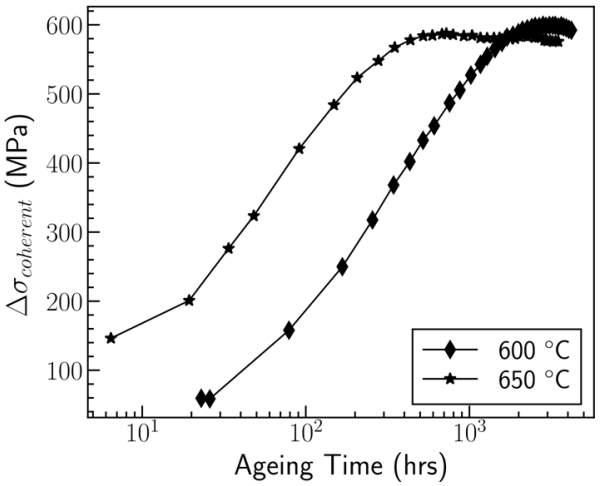

FIGURE 5: Coherent strength evolution in Inconel 625 aged at 600 ℃ and 650 ℃.

TABLE 2: Characterization of γ'' at instance of maximum $\sigma_{coherent}$. MS refers to the multistage aged samples.

Aging Temperature (℃)	Length (nm)	Thickness (nm)	Volume Fraction (%)	$\sigma_{coherent}$ (MPa)	Time (hrs)
600	23.3	8.3	5.9	599.4	2817.0
650	36.1	10.2	5.9	587.5	722.8

4. CONCLUSION

Using the phase-field and nucleation model, this study quantitatively investigates the precipitation kinetics of γ'' in Inconel 625. With model parameters from experimental calibrations, the phase-field results for microstructure, mean particle length, aspect ratio, and volume fraction evolution at different aging temperatures, compares favorably with experimental measurements. Additionally, utilizing the meso-

scale results from the phase-field simulations as input parameters to a macro-scale coherency strengthening model, the evolution of the yield strength during heat treatment was predicted. The current study provides a practical guidance for applying the phase-field approach as a link in the multiscale modeling of material properties.

ACKNOWLEDGEMENTS

This work is funded by the National Science Foundation (NSF), in United States under an award CMMI 1662854. The computer simulations were carried out on the clusters of High Performance Computing Collaboratory (HPC2) at Mississippi State University.

REFERENCES

[1] T. Gladman, "Precipitation hardening in metals," *Materials science and technology,* vol. 15, no. 1, pp. 30-36, 1999.

[2] R. Kampmann and R. Wagner, "Kinetics of Precipitation in Metastable Binary Alloys: Theory and Application to Copper--1. 9 at.% Titanium and Nickel--14 at.% Aluminium(Alloys)," *Decomposition of alloys: the early stages,* pp. 91-103, 1983.

[3] J. Svoboda, F. D. Fischer, P. Fratzl and E. Kozeschnik, "Modelling of kinetics in multi-component multi-phase systems with spherical precipitates: I: Theory," *Materials Science and Engineering: A,* vol. 385, no. 1-2, pp. 166-174, 2004.

[4] W. A. Johnson and R. F. Mehl, "Reaction kinetics in processes of nucleation and growth," *Transactions of the American Institute of Mining and Metallurgical Engineers,* vol. 135, pp. 396-415, 1939.

[5] L.-Q. Chen, "Phase-field models for microstructure evolution," *Phase-field models for microstructure evolution,* vol. 32, no. 1, pp. 113-140, 2002.

[6] X. Wang, P. Liu, Y. Ji, Y. Liu, M. Horstemeyer and L. Chen, "Investigation on microsegregation of IN718 alloy during additive manufacturing via integrated phase-field and finite-element modeling," *Journal of Materials Engineering and Performance,* vol. 28, no. 2, pp. 657-665, 2019.

[7] P. Liu, Z. Wang, Y. Xiao, R. Lebensohn, Y. Liu, M. Horstemeyer, X. Cui and L. Chen, "Integration of phase-field model and crystal plasticity for the prediction of process-structure-property relation of additively manufactured metallic materials," *International Journal of Plasticity,* vol. 128, p. 102670, 2020.

[8] W.-H. Yang, Z. Wang, C. Yenusah, and Y.-C. Liu, "An integrated model for prediction of process-structure-property relationship for additively manufactured Al-10Si-Mg alloy", SAE Technical Paper 2020-01-1075, 2020.

[9] H. Eiselstein and D. Tillack, "The invention and definition of alloy 625," *Superalloys 718,625 and Various Derivatives,* pp. 1-14, 1991.

[10] F. Zhang, *Ni-Nb-Al pseudo-ternary thermodynamic database,* Madison, 2010.

[11] J. W. Cahn and J. E. Hilliard, "Free energy of a nonuniform system. I. Interfacial free energy," *The Journal of chemical physics,* vol. 28, pp. 258-267, 1958.

[12] S. M. Allen and J. W. Cahn, "A microscopic theory for antiphase boundary motion and its application to antiphase domain coarsening," *Acta metallurgica,* vol. 27, pp. 1085-1095, 1979.

[13] J. P. Simmons, C. Shen and Y. Wang, "Phase field modeling of simultaneous nucleation and growth by explicitly incorporating nucleation events," *Scripta materialia,* vol. 43, pp. 935-942, 2000.

[14] E. Kozeschnik, I. Holzer and B. Sonderegger, "On the potential for improving equilibrium thermodynamic databases with kinetic simulations," *Journal of phase equilibria and diffusion,* vol. 28, pp. 64-71, 2007.

[15] I. J. Moore, *Modelling γ″ ($D0_{22}$) precipitate nucleation, growth and coarsening in the nickel-base superalloy 625,* PhD thesis: University of Sheffield, 2017.

[16] J. Oblak, D. Duvall and D. Paulonis, "An estimate of the strengthening arising from coherent, tetragonally-distorted particles," *Materials Science and Engineering,* vol. 13, no. 1, pp. 51-56, 1974.